ISSN 1330–0008
CODEN FIZAE4

HYPERSATELLITE AND SATELLITE TRANSITIONS IN SILVER ATOMS

VLADIMIR HORVAT* and KSENOFONT ILAKOVAC**

*Cyclotron Institute, Texas A&M University, College Station, TX 77843, USA[1]
**Department of Physics, Faculty of Science, University of Zagreb, POB 162, HR-41000 Zagreb, Croatia, and Ruđer Bošković Institute, 41000 Zagreb, Croatia

Received 9 December 1994

UDC 535.14

PACS 32.30.Rj, 32.70.Fw, 31.30.Jv

Previous measurements of the K X-rays emitted in the deexcitation of silver atoms with empty K-shells have been extended in order to obtain a better and more detailed quantitative description of the processes involved. The method of measurement has been improved and new data have been acquired. In addition, a more elaborate procedure for the analysis of data has been developed. In the analysis the complete set of peaks in the two-dimensional spectra originating from the hypersatellite-satellite cascades was treated in a self-consistent way. The Kα, K$\beta_{1'}$ and K$\beta_{2'}$ X-ray energy shifts caused by single K or $L_{2,3}$ spectator vacancies have been determined along with the intensity ratios $I(\mathrm{K}\alpha_2)/I(\mathrm{K}\alpha_1)$, $I(\mathrm{K}\beta_{1'})/I(\mathrm{K}\alpha_1)$ and $I(\mathrm{K}\beta_{2'})/I(\mathrm{K}\alpha_1)$ of the hypersatellite transitions (involving a K-shell spectator vacancy) and of the satellite transitions involving a single L_2 or L_3 spectator vacancy. The results are compared with the theoretical values.

1. *Introduction*

In 1916 Siegbahn and Stenström [1] discovered the lines in X-ray spectra that could not be explained on the basis of standard term diagrams. These lines were

[1]On leave of absence from the Physics Department, Faculty of Science, University of Zagreb

spectroscopically classified as non-diagram lines or X-ray satellites. In 1921 Wentzel [2] concluded that they originate from radiative one-electron transitions in atoms with more than one inner-shell vacancy. Since then these lines have been extensively studied both experimentally and theoretically. The satellite and hypersatellite spectra are very complex with many overlapping lines. The calculations of energies and transition probabilities are rather difficult because non-Coulomb interactions and relativistic effects strongly affect the results [3,4]. That means that accurate measurements of the energies and intensities of the satellites provide a sensitive test of the influence of various contributions to the atomic Hamiltonian. These include the Breit interaction, relativistic electron mass, interaction between magnetic dipole moments, retardation, electron self-energy, relaxation, vacuum polarization, correlation and the distribution of mass and charge inside the atomic nucleus.

One of the simplest configurations of an atom with more than one inner-shell vacancy is the K^{-2} configuration. In medium-heavy and heavy atoms it decays predominantly by the emission of a hypersatellite K X-ray in a transition in which an electron from a higher shell fills one of the K-shell vacancies. In this transition the other K-shell vacancy is called a spectator, even though its presence strongly affects the transition energies and branching ratios. The hypersatellite transition leads to an atomic configuration with one vacancy in the K-shell and one vacancy in the higher shell. It decays predominantly by the emission of a satellite K X-ray in a transition in which the other K-shell vacancy is filled. In this case the spectator vacancy is in the higher shell.

Pure K^{-2} configurations in atoms are most efficiently generated in nuclear decays in which the atomic vacancies are formed with high probability (such as the nuclear electron capture and electron conversion). The formation of single K-shell vacancies is most probable if the available transition energy is sufficient. The probability of forming two K-shell vacancies in the nuclear decay is very low and the probability of forming any additional vacancy is negligible. The processes which cause the ejection of an electron during a nuclear electron capture or electron conversion include direct collision of the captured or converted electron with one of the remaining atomic electrons, internal Compton scattering with electron conversion, electron conversion of internal bremsstrahlung and double electron conversion. However, experimental results indicate that the dominant mechanism involves the electron capture or conversion accompanied by the shakeoff or shakeup processes.

In the present work, the decay of radioactive ^{109}Cd atoms was used to generate the K^{-2} states in silver atoms. Its decay scheme is shown in Fig. 1 [5]. The nuclear electron capture decay (in which a K-electron is captured with a probability of 81.5 %) leads to the metastable state of ^{109m}Ag having a half-life of 39.8 s. The metastable state decays to the ground state by γ-emission or electron conversion. 41.7 % of the decays involve a K-electron. The K-electron capture and K-electron conversion processes produce K-shell vacancies independently from each other, since the half-life of the metastable state is very long when compared to the half-life of the K-shell vacancies and to the time resolution of the measurements. The probability of removal of both K-electrons (which is energetically allowed in both cases [5]) has been measured previously [6,7] and amounts to 6×10^{-5} per decay of ^{109}Cd.

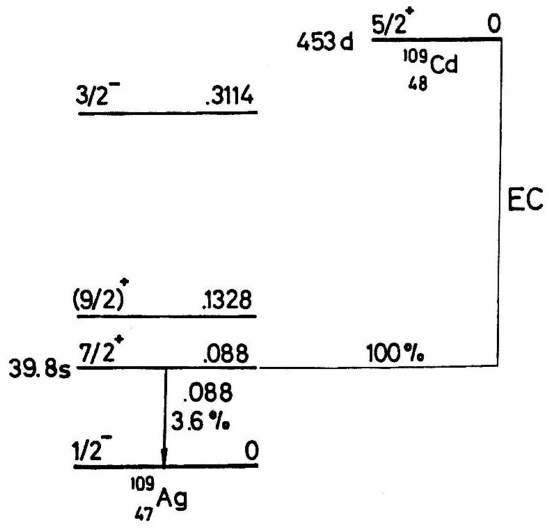

Fig. 1. Decay scheme of ^{109}Cd.

The two K X-rays can in principle be distinguished from each other and from the corresponding diagram K X-rays since they all have different transition energies. However, the difference between the transition energy of a satellite K X-ray and of the corresponding diagram K X-ray may in some cases be smaller then the energy resolution of the measuring apparatus. The application of the coincidence technique makes possible a very strong suppression of the very abundant ordinary (diagram) K X-rays, because they are randomly distributed in time. The decay of the K^{-2} states produces pairs of coincident K X-rays, the hypersatellite-satellite cascade, that are very efficiently recorded in the measuring system.

Earlier measurement of the hypersatellite shift of the Kα line has been made by van Eijk et al. [6].

This work represents an improvement and an extension of the similar measurements made earlier [7]. New results and smaller errors have been obtained by increasing the efficiency of the measuring apparatus, reducing the background and analyzing the collected data (including the data collected in the previous experiment) in a more refined way.

2. *Measurements*

The ^{109}Cd sources used in the measurements were prepared from radioactive $CdCl_2$ solutions (supplied by New England Nuclear, Boston, MA, USA). A small droplet of the solution was placed onto a polyethylene sheet and a small piece of pure cellulose paper was placed into the droplet. The paper was 0.1 mm thick and cut to a diameter of around 1 mm (initially 1.5 mm, and later downn to 0.4 mm diameter). After drying, it contained most of the radioactivity. Dried sources were sandwiched between two 0.6 mm thick polyethylene foils. Their initial strengths are listed in Table 1 along with other data pertinent to the measurements.

TABLE 1.

Data on measurements: average radioactivities of ^{109}Cd sources, I, solid angles of the detectors, Ω, source-to-detector distances, d, numbers of single K-shell vacancies generated in the sources, n_K, in the measurement times, t, and the coincidence efficiencies, ϵ_C. All measurements were made at 180^0, except for the one from column c, which was done at 130^0.

	Measurement								
	*/a	*/b	*/c	1	2	3	4	5	6
I/kBq	0.84	1.15	2.43	0.98	0.97	0.94	1.36	1.01	0.95
Ω/sr	0.77	0.77	0.43	1.59	1.59	1.59	1.68	1.48	1.48
d/mm	12.8	12.8	18.0	8.0	8.0	8.0	7.7	8.5	8.5
$n_K/10^9$	5.79	5.98	17.9	2.56	1.68	4.36	6.00	5.28	3.07
t/hours	1553	1172	1669	590	391	1047	995	1182	730
ϵ_C	0.85	0.86	0.89	0.93	0.93	0.92	0.87	0.87	0.92

*Three measurements of Ref. 6.

Two planar high-purity germanium detectors, that were used for the detection of X-rays, were placed in a cylindrical lead shield to reduce the background. A shield was also placed between the detectors to reduce the cross-talk. In the measurements at 180^0, the shield between the detectors was a double disc with a double-taper hole in the centre. Its thickness and composition varied from measurement to measurement. The thickness ranged from 2 to 13 mm, while the materials used included pure aluminium, pure brass, and aluminium with copper, brass and gold inserts. The diameter of double-taper holes was between 2 mm and 1.0 mm. A different shield was used in the measurements at 130^0. Its description has been given elsewhere [7], along with the description of the accompanying source holder. In each measurement at 180^0, the source was carefully centered in the double-taper hole in the shield. The shield with the source was subsequently placed inside the cylindrical lead shield, between the detectors.

The detectors were supplied by ORTEC, Oak Ridge, TN, USA. Nominal size of their sensitive volumes is 200 mm^2 x 7 mm thick. The thickness of the beryllium windows is 0.13 mm. A thorough check was made of detectors' performance [8] in order to determine their actual dimensions and sensitivities. At 5.9 keV the measured energy resolution was 230 and 210 eV, respectively, but at higher energies it ranged from about 260 eV at 9.876 keV (Kα X-ray of germanium) to about 310 eV at 22.162 keV (Kα_1 X-ray of silver).

Pulses from the detectors were fed into a fast-slow coincidence system with a three-parameter $128 \times 512 \times 512$ channel pulse-height analyzer [7]. For each coincidence event in the 250 ns range, the time difference (time channel, k_0) and the amplitudes of the pulses from the detectors (energy channels, k_1 and k_2) were measured. The data were stored event-by-event and analyzed off-line using mainframe and personal computers.

The measurements were performed in a series of runs, intermittently over a period of several years. A considerable effort has been put into the design of the apparatus in order to insure its stability. The stability was also checked on a regular basis. About 30 000 events were collected in each run (one record). The records were then organized into nine groups according to the sources and shields used, and taking into account the positions of characteristic peaks in each record. After the data from the first three groups have been collected and analyzed [7], the setup was changed to measure the decay of K^{-2} states in xenon atoms. In that work the experimental arrangement was optimized and the routines for the analysis of data were essentially improved [9]. The new methods were then applied to the following six groups of data related to the hypersatellite - satellite cascades in silver atoms.

3. Analysis of data

The three-parameter events were represented as points in a three-dimensional coordinate system, with one coordinate (k_0) representing the time difference, and the other two (k_1 and k_2) representing the X-ray energy channels. For each measurement, a time spectrum (projection onto the k_0 axis) was made of the section of the k_1-k_2 region comprising the peaks due to the hypersatellite-satellite cascades (ranging from approximately 21 keV to 27 keV on each energy axis). The time spectra consist of a very distinct peak (due to the real coincidences of hypersatellite-satellite cascades) and an almost constant background (due to the random coincidences of the much more numerous diagram K X-rays). The full with at half maximum of the peak (the time resolution) was typically between 9 and 14 ns. Only the events with k_0 channels in the peak region were considered in the final analysis. For the selected time channels, two-dimensional tables of numbers of counts (the $E_1 - E_2$ spectra) were constructed and analysed as described below. The selected range of time channels also determined the coincidence efficiency (see Table 1).

The numbers of counts in the peaks due to the hypersatellite-satellite cascades and other X-ray coincidences were determined from the $E_1 - E_2$ spectra by least-squares fitting. The fitting function was composed of 48 two-dimensional peaks, 8 ridges (bands) and a constant. Each peak was represented by a two-dimensional Gaussian function of variable widths. The numbers of counts in the tables were compared with the integrals of the fitting function over the channel limits. Out of the 48 peaks considered, 16 correspond to accidental coincidences of $K\alpha_1$, $K\alpha_2$, $K\beta_{1'}$, and $K\beta_{2'}$ diagram X-rays of silver, and 32 correspond to the real coincidences of $K\alpha_1$, $K\alpha_2$, $K\beta_{1'}$, and $K\beta_{2'}$ hypersatellite - satellite cascade K X-rays of silver. The numbers of counts in the peaks, which are symmetrical with respect to the exchange of k_1 and k_2, were assumed to be the same. This symmetry was carefully checked and proved to be very good. The bands were due to the accidental coincidences of K X-rays of silver with the continua below the full-energy peaks and to real coincidences of K X-rays of silver with bremsstrahlung radiation. There are several processes which are considered to contribute to the bremsstrahlung radiation spectrum. The most important contribution appears to come from the internal bremsstrahlung emitted during the electron capture decay of ^{109}Cd or by the converted electron in the decay of the 88 keV metastable state of ^{109}Ag. The shape of the spectrum of the bremsstrahlung radiation that is emitted in coincidence with diagram K X-rays of silver was represented by a constant divided by the energy (integrated over the channel limits). Such a parametrization proved to be very good. The background radiation level was very low. It was represented by the constant.

One variable parameter of the fit (a_1) represented the number of counts in the peak due to the random coincidences of Kα_1 X-rays (from two independent emissions of diagram Kα_1 X-rays, one being detected in each detector). The numbers of counts in the remaining 15 random-coincidence peaks were assumed to follow from the known intensity ratios of the diagram lines [5]: $I(\mathrm{K}\alpha_2)/I(\mathrm{K}\alpha_1) = 0.530$, $I(\mathrm{K}\beta_{1'})/I(\mathrm{K}\alpha_1) = 0.273$, and $I(\mathrm{K}\beta_{2'})/I(\mathrm{K}\alpha_1) = 0.050$.

TABLE 2.
Notation for the numbers of counts, n, in the two-dimensional peaks due to the hypersatellite-satellite cascades.

	Hypersatellite transitions							
	Kα_1^h		Kα_2^h		Kβ_1^h		Kβ_2^h	
Satel-	Kα_1L$_3^{-1}$	n_a	Kα_1L$_2^{-1}$	n_e	Kα_1M^{-1}	n_i	Kα_1N^{-1}	n_m
lite	Kα_2L$_3^{-1}$	n_b	Kα_2L$_2^{-1}$	n_f	Kα_2M^{-1}	n_j	Kα_2N^{-1}	n_n
trans-	Kβ_1L$_3^{-1}$	n_c	Kβ_1L$_2^{-1}$	n_g	Kβ_1M^{-1}	n_k	Kβ_1N^{-1}	n_o
itions	Kβ_2L$_3^{-1}$	n_d	Kβ_2L$_2^{-1}$	n_h	Kβ_2M^{-1}	n_l	Kβ_2N^{-1}	n_p

In the following the designation of the satellite K X-ray will be extended by the subshell of the spectator vacancy. E.g., Kα_1^sL$_3^{-1}$ will mean a satellite Kα_1^s X-ray in the presence of an L$_3$ spectator vacancy. The number of counts in the peaks (two peaks are observed because of symmetry of the apparatus) due to the Kα_1^h - Kα_1^sL$_3^{-1}$ hypersatellite-satellite cascade, n_a (see Table 2), was represented by the variable parameter a_2. The ratios of numbers of counts in the peaks due to the hypersatellite lines were the variable parameters a_3, a_4 and a_5. They were determined from the relations

$n(\mathrm{K}\alpha_2^h) = n_e + n_f + n_g + n_h = a_3(n_a + n_b + n_c + n_d)$,

$n(\mathrm{K}\beta_{1'}^h) = n_i + n_j + n_k + n_l = a_4(n_a + n_b + n_c + n_d)$, and

$n(\mathrm{K}\beta_{2'}^h) = n_m + n_n + n_o + n_p = a_5(n_a + n_b + n_c + n_d)$.

Three variable parameters were the ratios of numbers of counts in the peaks due to the satellite transitions in atoms with a single L$_3$ spectator vacancy:

$n_b = a_6 n_a$, $\quad n_c = a_7 n_a$ $\quad$ and $\quad n_d = a_8 n_a$.

Another three variable parameters were the ratios of numbers of counts in the peaks due to the satellite transitions in atoms with a single L$_2$ spectator vacancy:

$n_f = a_9 n_e$, $\quad n_g = a_{10} n_e$ $\quad$ and $\quad n_h = a_{11} n_e$.

The intensity ratio of the Kα_2^s and Kα_1^s transitions with a single M or N spectator vacancy was assumed to be equal to the corresponding ratio for the diagram lines, i.e., $n_j = 0.530 n_i$ and $n_n = 0.530 n_m$. This assumption was based on the fact that the screening effect from outer electrons does not affect considerably the inner-shell electrons. However, two variable parameters, a_{12} and a_{13} were introduced to take account of the ratios of numbers of counts of the K$\beta_{1'}$ and K$\beta_{2'}$ satellite transitions in atoms with with a single M or N spectator vacancy:

$n_k = a_{12} n_i$ and $n_l = a_{13} n_i$, and

$n_o = a_{12} n_m$ and $n_p = a_{13} n_m$.

Three variable parameters, a_{14}, a_{15} and a_{16} represented the energy shifts of K$\alpha^h_{1,2}$, K$\beta^h_{1'}$ and K$\beta^h_{2'}$ hypersatellite transitions, while another three variable parameters, a_{17}, a_{18} and a_{19}, represented the corresponding satellite shifts due to a single L_3 or L_2 vacancy.

K$\beta_{1'}$ satellite shifts due to the presence of an M or N spectator vacancy were fixed at 33 and 4.7 eV, respectively, and the K$\beta_{2'}$ satellite shifts due to the presence of an N spectator vacancy was fixed at the value of 11.6 eV [10]. It was found that the variations of these values do not affect significantly the final results for the shifts of the Kα, K$\beta_{1'}$, and K$\beta_{2'}$ lines due to the presence of single K or $L_{2,3}$ spectator vacancies, as determined in the fitting procedure. The remaining K X-ray satellite shifts (K$\alpha_{1,2}$ satellite shift due to the presence of an M or N spectator vacancy and K$\beta_{2'}$ satellite shift due to the presence of an M spectator vacancy) were determined from the other shifts using the fact that the total energy released in a cascade transition does not depend on the energy of the intermediate state. In the analysis of the real coincidences, only pairs of X-rays that are emitted in the transitions in which one immediately follows the other were considered. The possibility of the existence of intermediate transitions was neglected.

Four variable parameters corresponded to the energy points on the k_1 axis (a_{20} and a_{21}), and k_2 axis (a_{22} and a_{23}). These energy points were the positions of peaks due to the Kα_1 and K$\beta_{1'}$ diagram lines and served as reference points for the determination of the energy scales. One variable parameter was used to describe the amplitudes of the continuum bands (a_{24}), and another one to represent the constant background (a_{25}).

The energy-dependent detector efficiencies were determined dynamically in the course of the fitting procedure. The efficiency function of the detectors (which depends on the energy and angle of incidence [8,11]), multiplied by the (angle-dependent) factors due to the attenuation of radiation in the materials that are placed between the source and detector (cellulose, polyethylene, air and beryllium window) was integrated over the solid angle of the detectors subtended from the source. Tabulated best-fit parameters [12] were used to determine the necessary attenuation coefficients.

The values of the parameters were derived from the fit with equal weights, while the errors were derived from the fit with weights equal to the reciprocal numbers of counts (one for zero count [13]). The 25-variable-parameter fit was multiply checked to make sure that the results corresponded to the absolute minimum of the χ^2 variable. Modified fitting functions, with smaller or larger numbers of variable parameters, were also used. The number was reduced by fixing values of some variable parameters. Additional parameters were, for instance, the extrapolated widths of the peaks at zero energy and the slopes of the squares of the widths as the functions of energy. The results obtained were very consistent, i.e., the variations of the best-fit values of the parameters were within the statistical errors.

4. Results

Results of the first three measurements were reported in Ref. 6. They are given in Tables 3 - 8 in the columns marked with asterisks. For intensity ratios the numbers are different because the reference intensity was changed from $I(\mathrm{K}\alpha_{1,2})$ to $I(\mathrm{K}\alpha_1)$.

4.1. Energy shifts of the hypersatellite and satellite lines

Results of the measurements for the energy shifts of hypersatellite lines are shown in Table 3. Statistics in the six new measurements was sufficient to allow the determination of the shifts of the $\mathrm{K}\beta_{1'}$ and $\mathrm{K}\beta_{2'}$ hypersatellite lines. The results of the measurements for the energy shifts of the satellite lines in atoms with a single L_2 or L_3 spectator vacancy are shown in Table 4. The new measurements allowed also the determination of $\mathrm{K}\beta_{1'}L^{-1}$ and $\mathrm{K}\beta_{2'}L^{-1}$ satellite shifts, (i.e. the shifts of the $\mathrm{K}\beta_{1'}$ and $\mathrm{K}\beta_{2'}$ line due to the presence of an L_2 or L_3 spectator vacancy.

TABLE 3.
Results of the measurements for the energy shifts of the hypersatellite transitions in silver atoms (due to a K-shell spectator vacancy).

Energy shift	Measurement						
	*	1	2	3	4	5	6
$\Delta^h(\mathrm{K}\alpha_{1,2})$ (eV)	546 ±20	505 ±22	536 ±31	529 ±13	535 ±14	558 ±21	530 ±20
$\Delta^h(\mathrm{K}\beta_{1'})$ (eV)	fixed at 681.5	633 ±30	685 ±37	660 ±21	667 ±14	651 ±16	737 ±29
$\Delta^h(\mathrm{K}\beta_{2'})$ (eV)	fixed at 681.5	674 ±113	825 ±87	684 ±90	728 ±40	677 ±51	651 ±97

*Ref. 6.

Weighted average values of the hypersatellite and satellite shifts given in Tables 3 and 4 are presented in Table 5. Previous result, 532±6 eV, of van Eijk et al. for $\Delta(\mathrm{K}\alpha^h)$ and our result are in a very good agreement. For comparison, the results of theoretical calculations are also included in the table. Detailed and very elaborate calculations of Chen et al. [4] and the results calculated with the routine of Desclaux [14] seem to be most reliable. The routine of Liberman et al. [15] gave larger deviations. Also included are the results of our Dirac-Hartree-Slater calculations [16] and the results of Burch et al. [17].

TABLE 4.
Results of the measurements for the energy shifts of the satellite transitions in silver atoms with an L_2 or L_3 spectator vacancy.

Energy shift	Measurement						
	*	1	2	3	4	5	6
$\Delta^s(\mathrm{K}\alpha\mathrm{L}^{-1})$ (eV)	54.5 ±6.4	59.6 ±19	66 ±18	56.8 ±7.9	77 ±11	71.5 ±8.6	67 ±17
$\Delta^s(\mathrm{K}\beta_{1'}\mathrm{L}^{-1})$ (eV)	fixed at 153	110 ±31	94 ±32	141 ±20	147 ±13	127 ±17	156 ±27
$\Delta^s(\mathrm{K}\beta_{2'}\mathrm{L}^{-1})$ (eV)	fixed at 153	170 ±94	86 ±98	173 ±65	118 ±44	148 ±100	133 ±86

*Ref. 6.

TABLE 5.
Hypersatellite and satellite energy shifts in silver atoms (in eV*).*

Transition	Spectator vacancy	Results of	$\Delta(\mathrm{K}\alpha)$	$\Delta(\mathrm{K}\beta_{1'})$	$\Delta(\mathrm{K}\beta_{2'})$
Hyper-satellite	K^{-1}	Theory [4]	534.7	681.6	—
		Theory [14]	539	683	719
		Theory [15]	408	548	509
		Theory [16]	508	689	753
		van Eijk et al. [6]	532 ±6	—	—
		This measurement	533.6 ±6.8	666 ±11	711 ±26
Satellite	L^{-1}	Theory [17b]	67.3	153	—
		Theory [17a]	71.5	178	—
		Theory [14]	63	144	179
		Theory [15]	66	149	177
		Theory [16]	74	192	246
		This measurement	62.1 ±3.7	136.4 ±8.1	135 ±29

4.2. Intensity ratios of the hypersatellite and satellite lines

Results of the measurements for the intensity ratios $I(\mathrm{K}\alpha_2)/I(\mathrm{K}\alpha_1)$, $I(\mathrm{K}\beta_{1'})/I(\mathrm{K}\alpha_1)$ and $I(\mathrm{K}\beta_{2'})/I(\mathrm{K}\alpha_1)$ of the hypersatellite lines are given in Table 6. Similarly, the results for these intensity ratios but for the satellite lines due to the presence of a single L_3, L_2 and M or N spectator vacancy are given in Table 7, 8 and 9, respectively. As may be seen, the new measurements allowed the determination of the intensity ratio $I(\mathrm{K}\alpha_2)/I(\mathrm{K}\alpha_1)$ in the presence of a single L_3 or L_2 spectator vacancy.

TABLE 6.
Results of the measurements for the intensity ratios of the hypersatellite transitions in silver atoms.

Intensity ratio	Measurement						
	*	1	2	3	4	5	6
$\frac{I(K\alpha_2^h)}{I(K\alpha_1^h)}$	0.85 ±0.38	0.35 ±0.22	0.87 ±0.54	0.73 ±0.14	0.78 ±0.22	1.09 ±0.39	0.84 ±0.22
$\frac{I(K\beta_{1'}^h)}{I(K\alpha_1^h)}$	0.361 ±0.079	0.245 ±0.042	0.33 ±0.11	0.298 ±0.026	0.299 ±0.038	0.439 ±0.079	0.348 ±0.046
$\frac{I(K\beta_{2'}^h)}{I(K\alpha_1^h)}$	0.102 ±0.026	0.024 ±0.029	0.091 ±0.051	0.061 ±0.014	0.064 ±0.013	0.100 ±0.020	0.056 ±0.022

*Recalculated results of Ref. 6.

TABLE 7.
Results of the measurements for the intensity ratios of the satellite transitions in silver atoms with an L_3 spectator vacancy.

Intensity ratio	Measurement						
	*	1	2	3	4	5	6
$\frac{I(K\alpha_2 L_3^{-1})}{I(K\alpha_1 L_3^{-1})}$	fixed at 0.53	0.65 ±0.19	0.72 ±0.28	0.536 ±0.077	0.92 ±0.19	1.01 ±0.18	0.29 ±0.24
$\frac{I(K\beta_{1'} L_3^{-1})}{I(K\alpha_1 L_3^{-1})}$	0.233 ±0.024	0.274 ±0.044	0.292 ±0.090	0.248 ±0.023	0.380 ±0.043	0.216 ±0.024	0.239 ±0.043
$\frac{I(K\beta_{2'} L_3^{-1})}{I(K\alpha_1 L_3^{-1})}$	0.052 ±0.017	0.056 ±0.029	0.045 ±0.060	0.057 ±0.015	0.091 ±0.017	0.080 ±0.015	0.063 ±0.030

*Recalculated results of Ref. 6.

Weighted average values of the $I(\mathrm{K}\alpha_2)/I(\mathrm{K}\alpha_1)$, $I(\mathrm{K}\beta_{1'})/I(\mathrm{K}\alpha_1)$ and $I(\mathrm{K}\beta_{2'})$ $/I(\mathrm{K}\alpha_1)$ intensity ratios given in Tables 6, 7, 8 and 9 are presented in Table 10. It should be noted that the results do not give the overall intensity ratios, but rather the ratios under the experimental conditions: 180^0 geometry with solid angles given in Table 1. (The measurement at 130^0 has small effect on the results, because of the relatively small statistical weights). If the angular distributions of the cascades were known, the results given in Table 10 could be used to determine the overall intensity ratios.

TABLE 8.
Results of the measurements for the intensity ratios of the satellite transitions in silver atoms with an L_2 spectator vacancy.

Intensity ratio	Measurement						
	*	1	2	3	4	5	6
$\frac{I(K\alpha_2 L_2^{-1})}{I(K\alpha_1 L_2^{-1})}$	fixed at 0.53	0.79 ±0.42	0.37 ±0.19	0.30 ±0.12	0.75 ±0.16	0.56 ±0.11	0.54 ±0.78
$\frac{I(K\beta_{1'} L_2^{-1})}{I(K\alpha_1 L_2^{-1})}$	0.233 ±0.024	0.37 ±0.12	0.382 ±0.074	0.223 ±0.046	0.260 ±0.036	0.364 ±0.044	0.28 ±0.14
$\frac{I(K\beta_{2'} L_2^{-1})}{I(K\alpha_1 L_2^{-1})}$	0.052 ±0.017	0.044 ±0.096	0.063 ±0.060	0.047 ±0.035	0.033 ±0.020	0.036 ±0.024	0.053 ±0.119

*Recalculated results of Ref. 6.

TABLE 9.
Results of the measurements for the intensity ratios of the satellite transitions in silver atoms with an M or N spectator vacancy.

Intensity ratio	Measurement						
	*	1	2	3	4	5	6
$\frac{I(K\beta_{1'}(MorN)^{-1})}{I(K\alpha_1(MorN)^{-1})}$	0.237 ±0.031	0.36 ±0.12	0.42 ±0.16	0.322 ±0.072	0.283 ±0.040	0.208 ±0.044	0.26 ±0.10
$\frac{I(K\beta_{2'}(MorN)^{-1})}{I(K\alpha_1(MorN)^{-1})}$	0.041 ±0.020	0.005 ±0.108	0.103 ±0.109	0.047 ±0.048	0.018 ±0.022	0.055 ±0.027	0.000 ±0.066

*Recalculated results of Ref. 6.

TABLE 10.
Intensity ratios of the hypersatellite and satellite transitions in silver atoms.

Transition	Spectator vacancy	Results of	$\frac{I(K\alpha_2)}{I(K\alpha_1)}$	$\frac{I(K\beta_1)}{I(K\alpha_1)}$	$\frac{I(K\beta_2)}{I(K\alpha_1)}$
Hyper-satellite	K^{-1}	Theory [4]	0.746	0.225	0.0393
		This measurement	0.723 ±0.088	0.306 ±0.017	0.068 ±0.008
Satellite	L_3^{-1}	Theory [18]	0.707	0.375	0.073
		This measurement	0.629 ±0.085	0.249 ±0.017	0.068 ±0.007
Satellite	L_2^{-1}	Theory [18]	0.265	0.281	0.055
		This measurement	0.495 ±0.076	0.265 ±0.022	0.043 ±0.011

In Table 10 are also given the theoretical values of the intensity ratios. The results of the very elaborate calculations of Chen et al. [4] for the intensity ratio $I(\mathrm{K}\alpha_2^h)/I(\mathrm{K}\alpha_1^h)$ are in a very good agreement with our results, but the values for the ratios $I(\mathrm{K}\beta_{1'}^h)/I(\mathrm{K}\alpha_1^h)$ and $I(\mathrm{K}\beta_{2'}^h)/I(\mathrm{K}\alpha_1)$ are significantly smaller than our experimental values. Theoretical results for the intensity ratios for the satellite lines are based on the semiempirical rules of Benka and Watson [18]. As stressed by the authors, the rules are very approximate. However, they seem to follow the trends in the data reasonably well.

4.3. Conclusions

The deexcitation of silver atoms in the K^{-2} configuration by the emission of K X-ray hypersatellite-satellite cascades was studied. New results for the energy shifts of Kα, K$\beta_{1'}$ and K$\beta_{2'}$ lines due to the presence of a K spectator vacancy (hypersatellite shifts) and a single L spectator vacancy (satellite shifts) have been obtained. Relative intensities of the Kα_2, K$\beta_{1'}$ and K$\beta_{2'}$ lines with respect to the Kα_1 line for the transitions in the presence of single K, L_2 and L_3 spectator vacancies have also been determined.

Nuclear decay processes that cause the removal with high probability of an electron from the K-shell (the electron capture and electron conversion) cause also, but with very low probability, ejection of the other K-electron. Probability of ejection of yet another electron from a higher shell is extremely low. Therefore, the K^{-2} states produced in nuclear decay are very pure double-vacancy states.

With regard to theory, new calculations of the K X-ray transition probabilities in the presence of L spectator vacancies are needed. The same holds for the angular correlations of the hypersatellite-satellite cascades.

Acknowledgements

This work was partially supported by the Ministry of Science and Culture and by the Ministry of Education of the Republic of Croatia.

References

1) M. Siegbahn and and W. Stenström, Phys. Z. **17** (1916) 48;

2) G. Wentzel, Ann. d. Physik **66** (1921) 437;

3) B. L. Scott, Phys. Rev. A**34** (1986) 4438; J. P. Desclaux, Ch. Briançon, J. P. Thibaud and R. J. Walen, Phys. Rev. Letters **32** (1974) 447;

4) M. H. Chen, B. Crasemann and H. Mark, Phys. Rev. A**25** (1982) 391;

5) C. M. Lederer and V. S. Shirley, *Table of Isotopes, 7th ed.* (Wiley-Interscience, New York, 1978);

6) C. W. E. van Eijk, J. Wijnhorst and M. A. Popelier, Phys. Rev. C**19** (1979) 1047;

7) V. Horvat and K. Ilakovac, Phys. Rev. A**31** (1985) 1543;

8) K. Ilakovac, V. Horvat and N. Ilakovac, Nucl. Instr. and Methods **228** (1984) 210;

9) K. Ilakovac, M. Veskovi¸ V. Horvat and S. Kauči¸ Phys. Rev. A**42** (1990) 3984;

10) V. Horvat and K. Ilakovac, calculations based on wave functions of E. Clementi and C. Roetti, At. Data Nucl. Data Tables **14** (1974) 177; to be published;

11) M. P. Fioratti and S. R. Piermattei, Nucl. Instr. and Meth. **96** (1971) 605;

12) W. H. Mc Master, N. K. Del Grande, J. H. Mallet and J. H. Hubell, Lawrence Livermore Radiation Laboratory Report No. UCRL-50174, 1969 (unpublished);

13) P. R. Bevington, *Data Reduction and Error Analysis for the Physical Sciences* (McGraw-Hill, New York, 1969);

14) J. P. Desclaux, Computer Phys. Comm. **9** (1975) 31;

15) D. A. Liberman, D. T. Cromer and J. T. Waber, Computer Phys. Comm. **2** (1971) 107;

16) From DHS calculations using only the spherically symmetric Coulomb interaction for the Hamiltonian;

17) a) D. Burch, L. Wilets and W. E. Meyerhof, Phys. Rev. A **9** (1974) 1007; b) D. Burch H. Wolter and P. Richards, results quoted in reference a);

18) O. Benka and R. L. Watson, Phys. Rev. A**29** (1984) 2255.

HIPERSATELITSKI I SATELITSKI PRIJELAZI U ATOMIMA SREBRA

VLADIMIR HORVAT* i KSENOFONT ILAKOVAC**

**Cyclotron Institute, Texas A&M University, College Station, TX 77843, SAD*[2]
***Fizički odjel, Prir.-mat. fakultet Sveučilišta u Zagrebu, P. P. 162, HR-41000 Zagreb, Hrvatska, i Institut "Ruđer Boškovi¸", 41000 Zagreb, Hrvatska*

UDK 535.14

PACS 32.30.Rj, 32.70.Fw,31.30.Jv

Ranija mjerenja K rendgentskog zračenja koje nastaje u raspadu atoma srebra s praznom K ljuskom nastavljena su radi postizanja boljeg i detaljnijeg opisa uključenih procesa. Poboljšana je metoda mjerenja i sakupljeni su novi podaci. Također je razvijena bolja metoda analize podataka u kojoj se cjelokupan skup vrhova u dvodimenzijskim spektrima, koji su posljedica kaskadnih raspada hipersatelit–satelit, obrađuje na samosaglasan način. Određeni su pomaci linija Kα, K$\beta_{1'}$ i K$\beta_{2'}$ zračenja uzrokovani pojedinačnim K ili $L_{2,3}$ promatračkim šupljinama, te omjeri intenziteta hipersatelitskih linija (sa promatračkom šupljinom u K-ljusci) i satelitskih prijelaza sa šupljinom u L_2 ili L_3 podljusci. Rezultati su uspoređeni s teorijskim vrijednostima.

[2]Na dopustu sa Fizičkog odjela Prir.-mat. fakulteta Sveučilišta u Zagrebu.